Title

Wood-Inspired Morphologically Tunable Aligned Hydrogel for High-Performance Flexible All-Solid-State Supercapacitors

Journal

Advanced Functional Materials, 30(10)

ISSN

1616-301X

Authors

Zhao, Y
Alsaid, Y
Yao, B
et al.

Publication Date

2020-03-01

DOI

10.1002/adfm.201909133

Peer reviewed

ADVANCED FUNCTIONAL MATERIALS
www.afm-journal.de

Wood-Inspired Morphologically Tunable Aligned Hydrogel for High-Performance Flexible All-Solid-State Supercapacitors

*Yusen Zhao, Yousif Alsaid, Bowen Yao, Yucheng Zhang, Bozhen Zhang, Neel Bhuskute, Shuwang Wu, and Ximin He**

Oriented microstructures are widely found in various biological systems for multiple functions. Such anisotropic structures provide low tortuosity and sufficient surface area, desirable for the design of high-performance energy storage devices. Despite significant efforts to develop supercapacitors with aligned morphology, challenges remain due to the predefined pore sizes, limited mechanical flexibility, and low mass loading. Herein, a wood-inspired flexible all-solid-state hydrogel supercapacitor is demonstrated by morphologically tuning the aligned hydrogel matrix toward high electrode-materials loading and high areal capacitance. The highly aligned matrix exhibits broad morphological tunability (47–12 µm), mechanical flexibility (0°–180° bending), and uniform polypyrrole loading up to 7 mm thick matrix. After being assembled into a solid-state supercapacitor, the areal capacitance reaches 831 mF cm^{-2} for the 12 µm matrix, which is 259% times of the 47 µm matrix and 403% times of nonaligned matrix. The supercapacitor also exhibits a high energy density of 73.8 µWh cm^{-2}, power density of 4960 µW cm^{-2}, capacitance retention of 86.5% after 1000 cycles, and bending stability of 95% after 5000 cycles. The principle to structurally design the oriented matrices for high electrode material loading opens up the possibility for advanced energy storage applications.

1. Introduction

Various natural systems such as muscles, tendons, skins,[1] articular cartilage,[2] and wood[3] exhibit well-defined anisotropic structure. The high order of orientation plays a significant role in multiple functions, including mass transport, surface lubrication, and force generation.[4] Particularly, mass transport is greatly enhanced through vertically aligned channels due to the low tortuosity. Inspired by nature, considerable efforts focused on the design of aligned micrometer-scale porous structures, showing promising applications in electronics,[5,6] biomedical engineering,[7] and energy storage devices.[8,9] Solid electrolyte with aligned structures exhibits low tortuosity and thus facilitates high ionic transfer, comparable to bare liquid electrolyte. Such ordered structures have also been demonstrated to benefit particularly the rate capability in thick electrodes.[10,11] In addition, oriented porous structure provides continuous highways and sufficient surface area for high mass loading, which is desirable for lowering the manufacturing cost via inactive material reduction. As a pioneering example, Hu group reported an all-wood structured supercapacitor, showing high electrical conductivity, ionic conductivity, ultrahigh areal mass loading, and thus large areal capacitance.[12] However, wood has predefined channels with macro-pores and suffers from rigidity and lack of flexibility. It would be advantageous to possess mechanical flexibility and morphological tenability while maintaining all above superior electrochemical performance. Therefore, it is highly desirable to obtain a man-made anisotropic structure with similar or even smaller pores, owning high areal-mass loading and high flexibility for energy storage applications.

Hydrogels are porous soft materials comprised of cross-linked polymeric network with high water content.[13] They have become promising matrices for electrode materials and electrolyte in aqueous supercapacitors and batteries, due to the increasing demands for flexibility, wearability, and portability with minimized liquid leakage.[14] Specifically, hydrogel with 3D highly ordered structures further grants favorable anisotropic properties, such as enhanced directional ion transfer. Currently, anisotropic hydrogels are mainly synthesized through directional stimuli, including mechanical forces,[15] magnetic field,[16] electric fields,[17] directional freezing,[18] and directional ion diffusion.[19] Particularly, the directional-freezing, or ice-templating, is a promising and versatile approach to create well-defined aligned porous channels along the freezing direction.[20–22] In this process, the hydrogel precursor solution is frozen along a directional temperature gradient.[23] Meanwhile, the monomers are concentrated between crystalline domains and subsequently polymerized in the presence of ice. Since the ice crystals serve as the template for the cross-linked polymer structure, removal of ice leads to porous monoliths. By manipulating the temperature gradient, solution concentration,

Y. Zhao, Y. Alsaid, Dr. B. Yao, Y. Zhang, B. Zhang, N. Bhuskute, Dr. S. Wu, Prof. X. He
Department of Materials Science and Engineering
University of California, Los Angeles
Los Angeles, CA 90095, USA
E-mail: ximinhe@ucla.edu
Prof. X. He
California Nanosystems Institute
Los Angeles, CA 90095, USA
The ORCID identification number(s) for the author(s) of this article can be found under https://doi.org/10.1002/adfm.201909133.

DOI: 10.1002/adfm.201909133

viscosity, wetting properties and incorporating additives, the morphology can be facilely tuned.[24–26] However, the pore sizes created from directional freezing method are typically larger than 20 μm even under the most favorable conditions such as crystallization in liquid nitrogen, which limits their applications in energy storage.

Considerable fundamental studies have investigated anisotropic hydrogel structures serving for supercapacitor electrolytes. The Wang group fabricated aligned poly(ethylene glycol) monomethacrylate ionogel,[20] poly(*N*,*N*-dimethylacrylamide) (PDMAA) ionogel,[21] and polyacrylamide (PAAm) gel[22] as gel electrolytes through directional freezing. With the same electrodes covering both sides of the gel electrolyte, the device with anisotropic structure presented improved ionic conductivity and enhanced specific capacitance at high current in comparison to the isotropic, nonaligned gel. With aligned architecture, the supercapacitor energy loss was significantly reduced.[21] Notably, the electrochemical performance with aligned structure was comparable to that of a pure electrolyte device.

In addition to the electrolyte, the structural design of the overall device is important for energy storage devices with high mass loading, low tortuosity, and high energy/power density. Conventionally, electrode materials are coated on the surface of electrolyte, which limits the ion transport. To maintain high specific capacitance, the electrode mass loading is kept low; however, the low mass loading inevitably results in low total areal capacitance and increases the fraction of nonenergy storage, inactive materials, which is undesirable for practical energy storage devices.[10] For example, hierarchical aligned nanomaterials based on transition metal oxides/sulfides have displayed outstanding specific capacitance due to the high specific area. A few conducting polymers with nanostructure have also been studied, including poly(3,4-ethylenedioxythiophene)-polystyrene sulfonate,[27] polyaniline (PANi),[28] and polypyrrole (PPy).[29] However, it still remains a big challenge to efficiently and cost-effectively fabricate the materials with high areal energy density and high mass loading (**Table 1**).[30,31] One route to address the ion-transport issue while maintaining the high mass loading is to embed electrode materials in the porous electrolyte matrix. By controlling the morphological orientation and size distribution of the porous matrix, the electrode materials loading can also be optimized, which can effectively improve the device electrochemical performance.

Here, we demonstrate a wood-inspired all-solid-state hydrogel supercapacitor by integrating PPy as the electrode material in an aligned polyacrylamide aerogel (APA) matrix. The PAAm hydrogel with unidirectionally aligned structure was created using an ice-templating method featuring highly controllable and tunable morphology and good mechanical flexibility. The anisotropic structure enabled ions to freely travel through the channels due to the low tortuosity. The electroactive material PPy was subsequently embedded inside the aligned-structured aerogel film by vapor-phase deposition (VPD), to form a complete flexible all-polymer electrode. The unidirectional and open microchannels generated by directional freezing allowed pyrrole molecules to freely penetrate the PAAm matrix, showing homogenous distribution of PPy up to 6.7 mm thickness of APA. When two PPy-embedded aligned-PAAm electrodes were soaked with polyvinyl alcohol (PVA)/LiCl electrolyte and sandwiched with a cellulose-based separator, an all-solid-state supercapacitor was formed. Uniquely, the electrode and electrolyte share a same porous polymer matrix to form interconnected network, in which gel electrolyte provides good mechanical flexibility as well as fast ion transfer, and PPy exhibits charge storage capability and chemical stability. These merits are attributed to such an integrated electrode/electrolyte design as proven previously.[32] Additionally, the porous matrix increases the mass loading of the electroactive material (PPy here). Importantly, the aerogel pore size can be further drastically reduced from 47 to 12 μm simply by adding PVA to the precursor solution, successfully producing a larger specific area desirable for high supercapacitor performance. The areal capacitance reached 831 mF cm^{-2} at 6.2 mA cm^{-2} for the 12 μm pore matrix, which is 259% of capacitance of the 47 μm pore matrix. The PPy/APA supercapacitor exhibited a high energy density of 73.8 μWh cm^{-2}, power density of 4960 μW cm^{-2}, capacitance retention of 86.5% after 1000 cycles at 6.2 mA cm^{-2}, and bending stability of 95%

Table 1. Comparison of solid-state supercapacitors based on hierarchical electrode materials and conducting polymer.

	Areal Capacitance	Energy density	Power density	Stability	Refs.
V_2O_5/rGO	207.9 mF cm^{-2}	73.9 μWh cm^{-2}	3770 μW cm^{-2}	65% retention after 8000 cycles	[30]
CuO	543 mF cm^{-2} at 7.5 mA cm^{-2}	19.7 mWh g^{-1}	700 mW g^{-1}	96% retention after 3000 cycles	[49]
PEDOT/PVA	66 mF cm^{-2} at 0.29A g^{-1}	15.2 mWh g^{-1}	201.1 mW g^{-1}	89% retention after 1000 cycles	[27]
PPy/PVA	152 mF cm^{-2} at 0.1 mA cm^{-2}	23.2 μWh cm^{-2}	1200 μW cm^{-2}	86.3% retention after 10 000 cycles	[32]
PPy/GO	152 mF cm^{-2} at 10 mV s^{-1}	12.9 μWh cm^{-2}	5760 μW cm^{-2}	88.3% retention after 10 000 cycles	[44]
PANi/steel	19 mF cm^{-2} at 0.32 mA cm^{-2}	0.95 μWh cm^{-2}	4200 μW cm^{-2}	100% retention after 10 000 cycles	[48]
CNT/GO/Ppy	72.3 mF cm^{-2} at 0.5 mA cm^{-2}	6.3 μWh cm^{-2}	3700 μW cm^{-2}	87.7% retention after 10 000 cycles	[46]
Graphene/PANi	23 mF cm^{-2} at 0.1 mA cm^{-2}	1.5 μWh cm^{-2}	1000 μW cm^{-2}	100% retention after 2000 cycles	[47]
Graphite/PANi	77.8 mF cm^{-2} at 0.1 mA cm^{-2}	7 μWh cm^{-2}	1180 μW cm^{-2}	83% retention after 10 000 cycles	[45]
All-in-one PANi/PVA	488 mF cm^{-2} at 0.2 mA cm^{-2}	42 μWh cm^{-2}	160 μW cm^{-2}	90% retention after 7000 cycles	[28]
All-in-one PPy/PVA	225 mF cm^{-2} at 0.8 mA cm^{-2}	20 μWh cm^{-2}	600 μW cm^{-2}	92% retention after 2000 cycles	[29]
PPy-SDS/PVA	950 mF cm^{-2} at 1.6 mA cm^{-2}	62.1 μWh cm^{-2}	570 μW cm^{-2}	84% retention after 1000 cycles	[43]
Our works	831 mF cm^{-2} at 6.2 mA cm^{-2}	73.8 μWh cm^{-2}	4960 μW cm^{-2}	86.5% retention after 1000 cycles	

after 5000 cycles. The capacitance performance was further improved to over 1838 mF cm^{-2} at 6.2 mA cm^{-2} at higher PPy loading and larger device thickness. Electrodes made of aligned aerogel matrices with loaded electrode materials open the possibility for highly tunable structural design for advanced energy storage applications.

2. Results and Discussion

2.1. Synthesis Methods of Aligned Aerogel

The aligned hydrogel matrix in this work is mainly comprised of chemically crosslinked polyacrylamide, polymerized from acrylamide as monomer, *N,N'*-methylenebis(acrylamide) (MBA) as crosslinker, ammonium persulfate (APS) as thermal initiator, and *N,N,N',N'*-tetramethylethylenediamine (TEMED) as catalytic agent (**Figure 1**). During the ice-templating process, the prepolymer components in suspension were well mixed and transferred to the mold. The mold was specifically designed with hollow side walls for thermal insulation, enabling the air in between to effectively inhibit the conduction of heat from the side walls into the solution (**Figure 2**a). Thus, the temperature gradient was preferably along the vertical direction. As the ice was nucleated and grown from the bottom to the top surface, the solutes were expelled to the region between the ice crystals. Then the sample was placed in −20 °C fridge for cryopolymerization.

The initiator APS and the catalyst TEMED were controlled as appropriate so that the polymerization predominantly occurred after the ice was completely formed; overly high APS and TEMED content would dramatically increase the reaction kinetics, leading to isotropic hydrogel without alignment,[24] as shown in Figure S1 in the Supporting Information. In addition, small amount of ethanol was added into the solution to modify the ice formation and mechanical robustness.[33] It is worth noting that the APA without ethanol formed cracks with poor mechanical strength (Figure S2a, Supporting Information). After the ice formation and cryopolymerization, the frozen sample was placed in a freeze-dryer to remove the ice. Then, the aligned aerogel film was formed. The APA displayed well-defined anisotropic structure along the freezing direction over

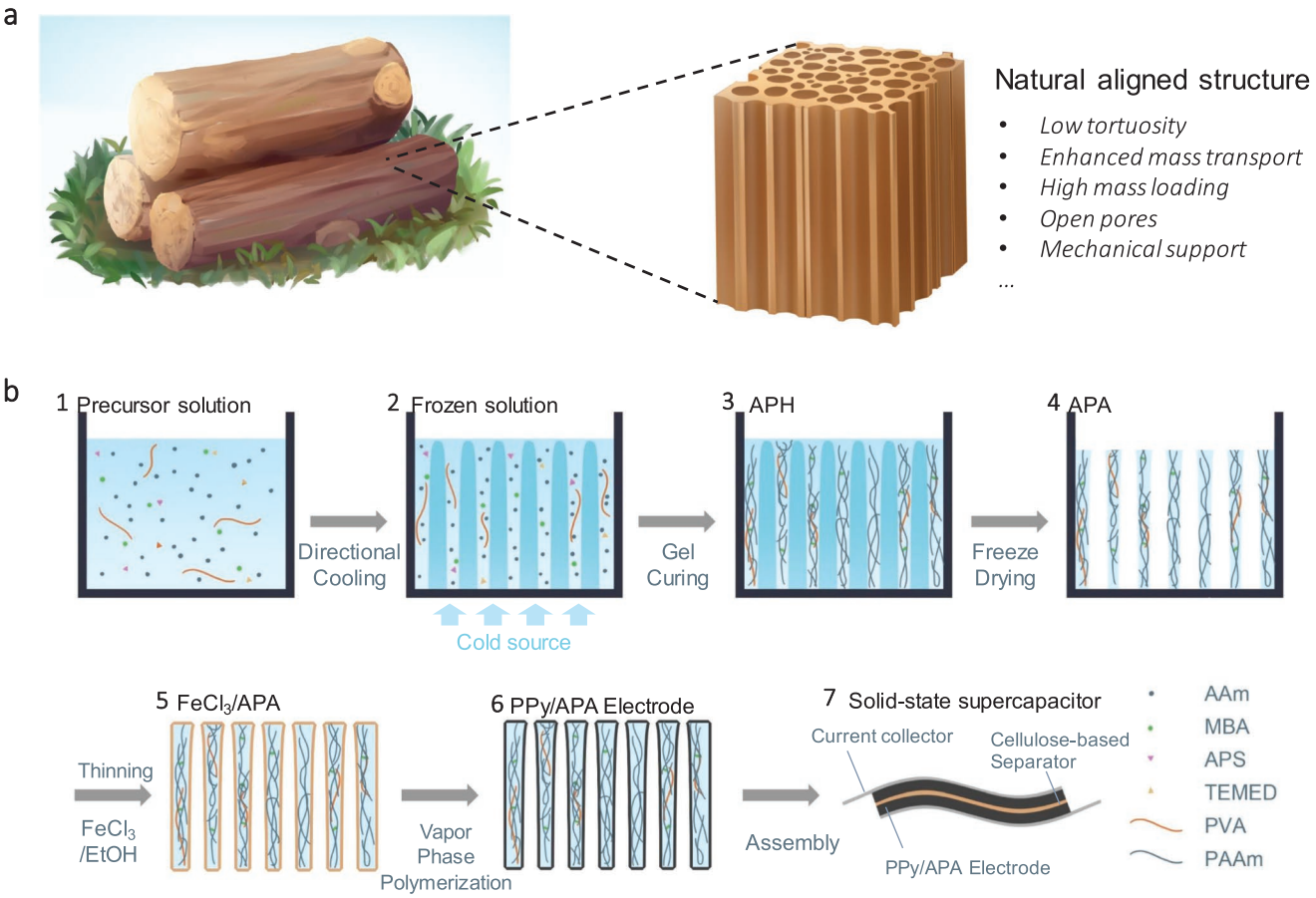

Figure 1. Schematic of the fabrication of all-solid-state hydrogel supercapacitors via integration of APA as the matrix and PPy as the electrode material. a) The precursor aqueous solution containing AAm, PVA, APS, TEMED, PVA, and a small amount of ethanol in water. b) Directional freezing of ice is carried out from the bottom to the top of the mold, during which the precursor reagents are excluded between the ice crystals. c) The AAm monomer is in situ cryopolymerized into PAAm hydrogel with well-defined aligned structure. d) The water is removed by freeze-drying under −50 °C and reduced pressure. e) The formed dry aerogel is sanded to a desired thickness and immersed in $FeCl_3$/ethanol solution. f) The $FeCl_3$-coated aerogel is dried and followed by VPD of PPy with pyrrole monomer under vacuum. g) The PPy/APA films are soaked in PVA/LiCl electrolyte solution, taken out, and assembled into sandwich-like supercapacitors with a separator.

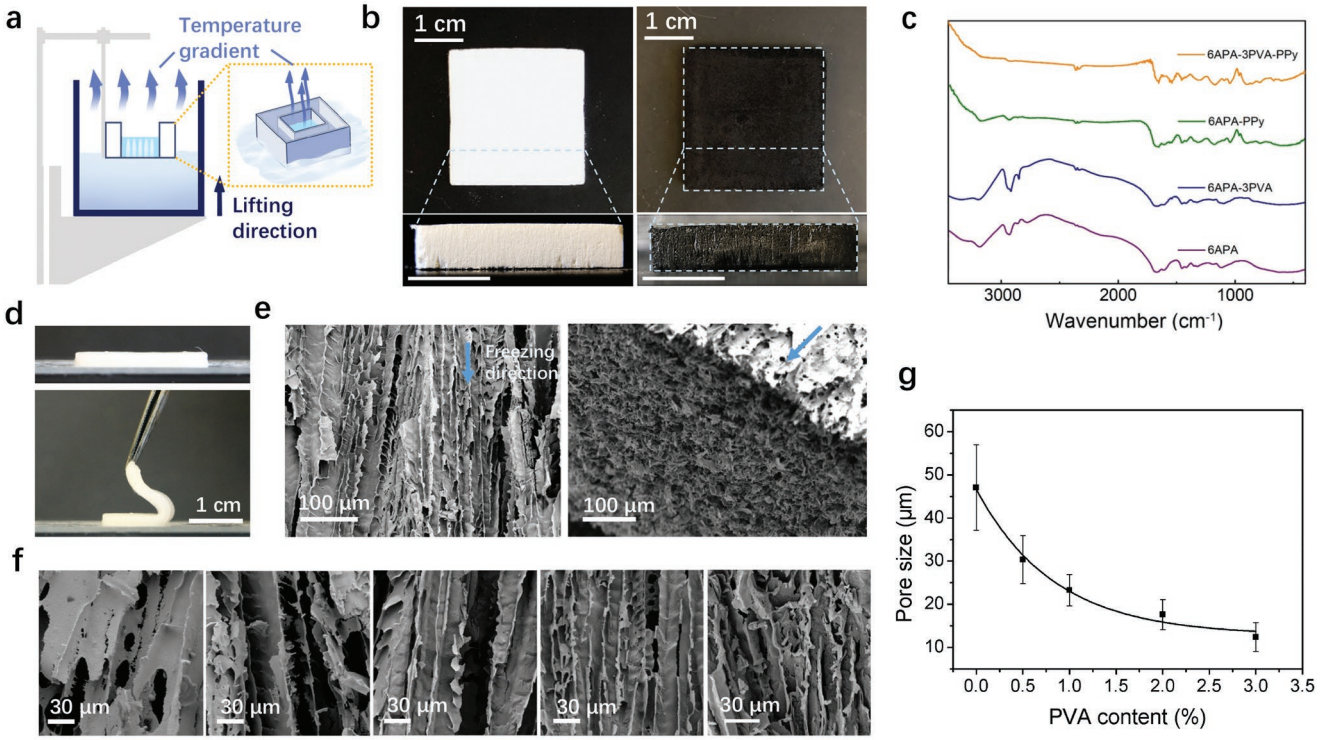

Figure 2. Morphology and materials characterization of PPy/APA film. a) Schematic of directional freezing setup. The inset shows the mold which remains hollow in between the inner precursor solution and outer liquid nitrogen, enabling the preferably vertical temperature gradient. b) Photographs of freeze-dried APA film (left) and PPy/APA film after the VPD (right). The PPy can facilely infiltrate into the matrix (up to 6.7 mm thick), attributed to the open porous structure along the aligned direction. c) FTIR spectra of APA and PPy/APA, with and without PVA addition. d) Photographs of swollen APA film on side view (upper) and its high flexibility capable of bending to a large angle (lower). e) SEM images of APA cross-sections, respectively, along the alignment (freezing) direction (left) and the transversal direction (right). f) SEM images of 6% PAAm containing 0, 0.5, 1, 2, and 3 wt% PVA. g) Tunability of the pore size of APA by tuning the PVA content in the precursor solution.

large scale (Figure 2e). After swelling in water, the APA film was flexible and capable of freely bending to large angles, demonstrating the potential for the flexible substrate (Figure 2d).

2.2. Morphology Control of Matrix

A small amount of PVA was added to prepolymer solution to control the morphology of the hydrogel/aerogel.[34] For ice-templating, the porosity of the materials is a replica of the original ice structure. By modifying the ice crystallization, we achieved a wide tunability of pore morphology of hydrogel. Here, the pore sizes of the aligned structure were facilely tuned by adding different concentration of PVA (Figure 2f). In Figure 2g, the APA without adding PVA had pore sizes of 47 µm. Whereas, the APA containing PVA from 0.5 to 3.0 wt% resulted in finer pores with higher PVA content. The smallest pores were 12 µm for 3.0 wt% of PVA, which was far lower than the channel width of wood (20–40 µm) and conventional directional freezing pores (>20 µm). The ability of effectively modifying the micromorphology by the PVA addition is due to the increased solution viscosity and hydrophilicity.[34] In addition, the PVA can inhibit the ice recrystallization during the gel curing step, which is an unavoidable annealing process.[35] Although adding more PVA is expected to further reduce the pore size, it increases the fraction of electrochemically inactive materials in the electrode and results in more zig-zag ice crystallization due to overly fast ice formation,[36] both not favorable for optimal supercapacitor behavior. Hence, 3.0 wt% was found to be the optimum PVA additive concentration in this material system.

2.3. PPy Loading

In recent years, several works have focused on improving electrochemical performance via structural design of electrode and electrolyte materials.[12,37] A larger specific surface area can be achieved by reducing the matrix pore sizes of the matrix. Therefore, when coating the same thickness of electrode materials on the matrix surface, finer structured matrix can accommodate more electroactive materials as coating due to the higher specific surface area.

We used PPy as an exemplary electrode material to demonstrate the structure tunability and electrochemical improvement due to its high conductivity, electrochemical properties, and facile fabrication.[32] To embed PPy in the substrate, the APA film was immersed in a $FeCl_3$/ethanol solution to coat oxidant throughout the entire matrix (Figure S3b, Supporting Information). After drying the film, it was exposed to pyrrole vapor by VPD. The PPy in the APA film was evenly grown on the inner channel walls (Figure S4a, Supporting Information). In addition, the PPy was homogenously distributed throughout the

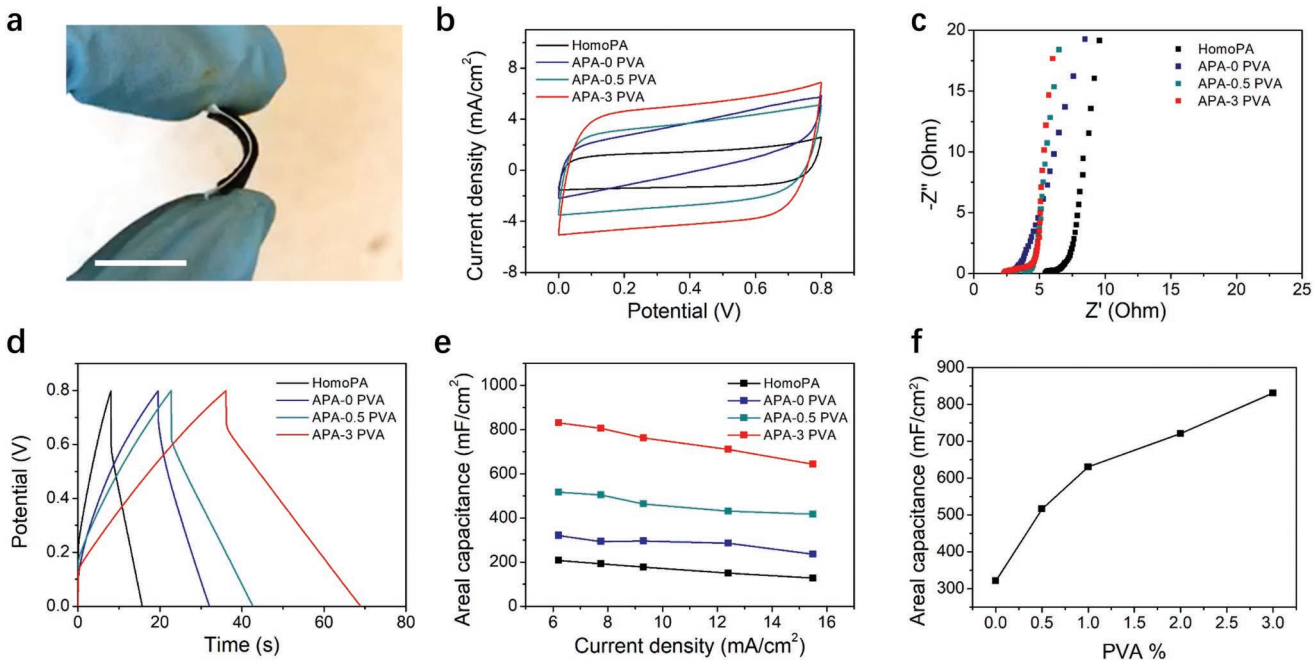

Figure 3. Electrochemical performance of supercapacitors with different matrix morphologies. a) Photograph of a flexible all-solid-state hydrogel supercapacitor. b) CV curves of the supercapacitors at the scan rate of 10 mV s^{-1}. The neat PAAm, PAAm with 0.5 wt% PVA, and PAAm with 3 wt% PVA were selected as the hydrogel matrix. c) Nyquist plots of the three supercapacitors at frequencies ranging from 1M to 0.01 Hz. d) GCD curves at the current density of 9.3 mA cm^{-2}. e) The correlation of areal capacitance with various current density. f) The areal capacitance of supercapacitors as the function of PVA additive concentration. The current density was 6.2 mA cm^{-2}.

entire film even up to 6.7 mm thickness (Figure 2b), showing significantly improved uniformity compared to previous methods with 10–100 µm penetration depth,[28,29,38] indicating the formation of a truly interpenetrating network of PPy/APA. The ice-templating method creates appropriate open macroporous pores with orientation, which not only supports the network from being collapsed when drying, but also provides sufficient space for gas molecule diffusion, in contrast with most previous close-pore structures.[39,40]

The chemical structures of pristine APA, APA with addition of PVA, and the aerogel after coating with PPy were analyzed using the Fourier transfer infrared (FTIR) spectra (Figure 2c). All the four samples had the peak at ≈3185 and ≈3327 cm^{-1}, which could be assigned to the characteristic peaks of N−H bonds.[41] The strong peak at ≈1650 cm^{-1} was derived from C=O stretching of the amide group, confirming the formation of PAAm structure. The peak at 1093 cm^{-1} from 6APA-3PVA was observed due to the C−O vibration of PVA. For 6APA-PPy and 6APA-3PVA-PPy which were coated with PPy by VPD, the absorption peak at ≈1548 cm^{-1} was attributed to the in-plane bending of C=N bonds. The peaks located at ≈1176 and ≈902 cm^{-1} were due to the stretching vibration of C−N^+ bonds and C=N^+−C bonds, confirming the formation of PPy.[42]

To examine the morphology dependency of the aerogel film electrochemical performance, we prepared PPy/APA films with different PVA concentrations under the identical VPD condition. An isotropic, nonaligned PAAm aerogel was also fabricated as a control sample (Figure S5, Supporting Information). Typically, the PPy was polymerized on the APA matrices which had a constant thickness (1 mm) and were soaked with $FeCl_3$/ethanol of the same concentration (14 w/v%). After the polymerization of PPy on the APA film and removing the excess monomer with an ethanol rinse, the film was immersed in LiCl/PVA aqueous electrolyte and dried in air to remove the excess water. Then, we assembled two electrode layers with a separator to construct a sandwich-like solid-state supercapacitor (**Figure 3**a). Two carbon cloths were used to cover the two sides of electrode to connect with the electrochemical instrument.

2.4. Electrochemical Performance of Solid-State Supercapacitors

The electrochemical properties of solid-state supercapacitors were measured as shown in Figure 3. The cyclic voltammetry (CV) curves of devices made from PPy/APA matrices with different pore sizes (APA-x PVA, x = 0, 0.5, 3 wt% PVA) and nonaligned, homogenous matrix (HomoPA), respectively, were measured at 10 mV s^{-1}. As shown in Figure 3b, all four CV curves demonstrated a nearly rectangular shape, indicating a fast and efficient ion transfer.[32,43] The enclosed CV area for the APA devices increased with decreasing pore size, an indication of higher loading of electrode materials. By contrast, supercapacitors made from a nonaligned matrix had the smallest enclosure area. For APA-3 PVA, the small equivalent series resistance (ESR = 6.1 Ω cm^2) and charge transfer resistance (R_{CT} = 1.3 Ω cm^2) in the Nyquist plots indicated a low ohmic contact between the electrode and electrolyte, as well as an enhanced ion transfer. The low ESR and R_{CT} of the PPy/APA

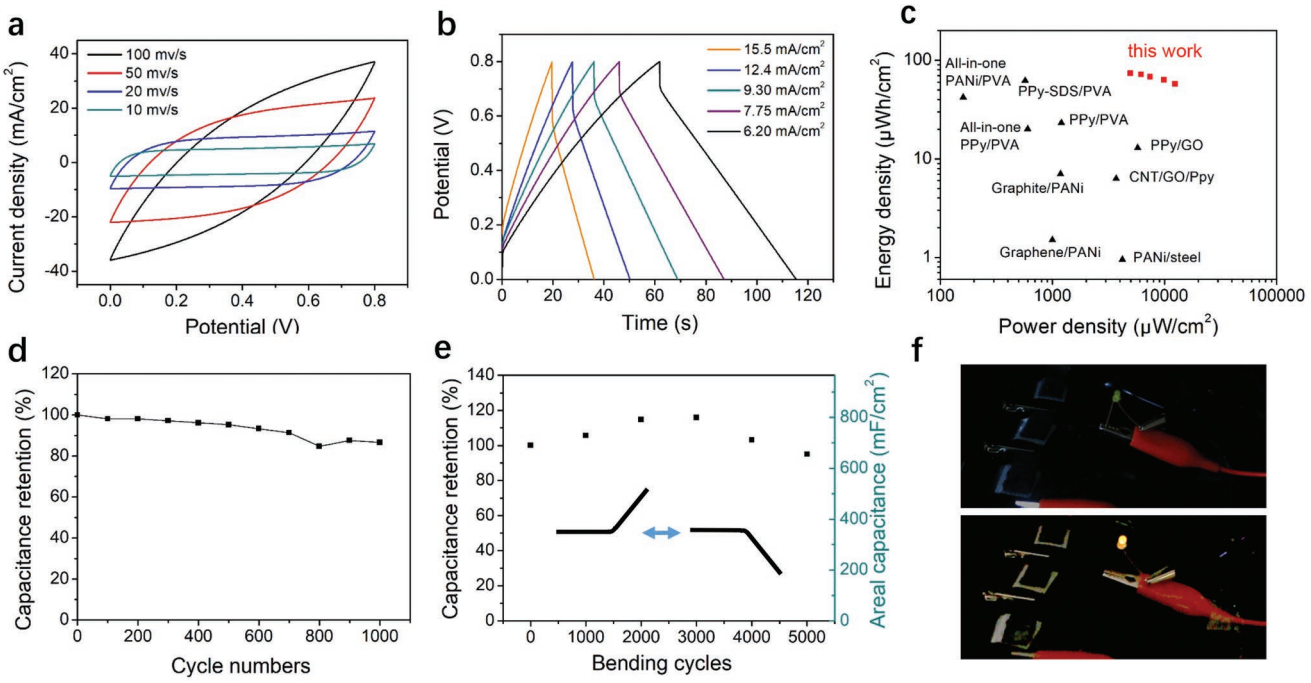

Figure 4. Electrochemical performance of the supercapacitor using PAAm hydrogel matrix containing 3 wt% PVA. a) CV curves at various scan rates from 10 to 100 mV s^{-1}. b) GCD curves at various current densities from 6.2 to 15.5 mA cm^{-2}. c) Ragone plots comparing this supercapacitor with other representative flexible all-solid-state supercapacitors, including PPy/PVA,[32] sodium dodecyl sulfate-modified PPy/PVA,[43] all-in-one PANi/PVA,[28] all-in-one PPy/PVA,[29] PPy/GO (graphene oxide),[44] graphite/PANi,[45] carbon nanotube/GO/PPy,[46] graphene/PANi,[47] and PANi/stainless steel wire.[48] d) Capacitance retention during 1000 charging–discharging cycles at current density of 6.2 mA cm^{-2}. e) Capacitance retention after 5000 repeated folding cycles. f) Demonstration of connecting three supercapacitors in series to light up a yellow LED.

electrode benefited from the aligned structure with low tortuosity that allowed for fast ion transport and defined electrical conduction pathways along channel walls. The nearly vertical tail at low frequency in the electrochemical impedance spectroscopy (EIS) plot also indicated favorable capacitive behavior. The galvanostatic charging–discharging (GCD) curves were measured with a current density of 9.3 mA cm^{-2} with an operating window of 0–0.8 V. Discharging time of the assembled supercapacitors was longer for smaller pore-sized devices, indicating larger areal capacitance (Figure 3f). In addition, the specific areal capacitance at various current densities were shown in Figure 3e, which were calculated from GCD tests. The HomoPA device had an areal capacitance of only 207 mF cm^{-2} at 6.2 mA cm^{-2}, whereas APA-PVA devices all exhibited much larger capacitance throughout the operational current range compared to HomoPA. For the matrix with 12 μm channels (APA-3 PVA), the areal capacitance reached 831 mF cm^{-2} at 6.2 mA cm^{-2} (332.4 F g^{-1}), 259% of the aerogel matrix without PVA addition (47 μm channel width) due to the morphology modification. The high capacitance is attributed to the reduction of microchannels width by morphological control of aerogel matrix.

We then focused on PPy/APA with 12 μm channels in further characterization due to its high performance. As shown in **Figure 4**a, the shape of CV diagrams at different scan rates (10–100 mV s^{-1}) was nearly symmetric, indicating a good capacitive behavior. The symmetry, triangular shape of GCD curves also demonstrates capacitive properties (Figure 4b). Benefiting from the large mass loading and thick electrode materials, the electrochemical test of the device had current density range of 3.1–15.5 mA cm^{-2} (Figure 4b and Figure S6, Supporting Information), which was considerably larger current value compared to state-of-the-art hydrogel supercapacitors (0.01–1 mA cm^{-2} in Table 1). Figure 4c illustrates the energy density (*E*) and power density (*P*) of such a solid-state supercapacitor, calculated from the GCD curves at different current densities. The largest areal energy density could reach 73.8 μWh cm^{-2} with an areal power density of 4960 μW cm^{-2}. As the areal power increased to 12 400 μW cm^{-2}, the areal energy density was still retained at 57.2 μWh cm^{-2}. The Ragone plots (Figure 4c) compare this device with previously reported state-of-the-art solid-state supercapacitors, presenting its outstanding performance of both high energy density and power density. In addition, the supercapacitor also possessed a high capacitance retention of 86.5% of its original capacitance after 1000 charging–discharging cycles at current density of 6.2 mA cm^{-2} (Figure 4d). The EIS after the cyclic stability test showed a slight shift, indicating the relatively small swelling of hydrogel and change in conductivity (Figure S7, Supporting Information). The PPy/APA supercapacitor not only exhibited high capacitance but also displayed excellent flexibility under bending, though the device (Figure 3a) had larger thickness than the conventional thin-film design. Figure 4e showcases the good capacitance retention under repeated bending of 90°. Interestingly, the capacitive performance was initially increased to ≈118% of its original capacitance and remained 95% after 5000 bending cycles. We attribute the initial performance enhancement under bending to the improved infiltration

of electrolyte into electrode under mechanical deformation. In addition, we connected three PPy/APA supercapacitors in series and successfully lit a yellow light-emitting diode (LED) bulb for over 250 s, suggesting promising applications for energy storage devices.

Directional freezing to prepare porous matrices combined with VPD polymerization to coat electrode materials (PPy) enable the versatile design of even larger areal capacitance devices. Using APA with 12 μm channels, we increased the oxidant agent $FeCl_3$ from 14 to 28 w/v%. The device exhibited low series resistance (≈4 Ω) and high areal capacitance of 1131 mF cm^{-2} at 6.2 mA cm^{-2}, shown in Figure S9 in the Supporting Information. Other than the increase in the content of oxidant agent, we also increased the original thickness of APA matrix from 1 to 2 mm to directly embed more PPy per unit area. Based on the 2 mm APA/PPy electrode with 3 wt% PVA and 28% $FeCl_3$/ethanol solution, the resultant areal capacitance was boosted to 1838 mF cm^{-2} at 6.2 mA cm^{-2}, shown in Figure S10 in the Supporting Information. To the best of our knowledge, this capacitance is among the highest of hydrogel-based solid-state supercapacitors.[28,29,32,43–48] Therefore, this presents a promising strategy that the morphological designs of anisotropic matrices and electrode materials coating can possibly advance energy storage devices and technologies.

In summary, we have established a new method of creating hydrogel of highly aligned microstructures with tunable fine features and high loading of electrochemical materials. Such a novel method successfully achieved a wood-inspired all-solid-state flexible supercapacitor with an integrated electrode/electrolyte design and significantly enhanced performance. It has the aligned polyacrylamide as the hydrogel matrix and PPy as the electrochemical material. The aligned polyacrylamide hydrogel exhibits low tortuosity, high ionic and electronic conductivity, and flexibility. By modifying the aligned hydrogel with the addition of hydrophilic PVA, the microchannel widths can be drastically reduced from 47 to 12 μm, resulting in 259% enhancement in areal capacitance. This value is higher than that of supercapacitor using homogenous matrix (HomoPA). The aligned supercapacitors exhibit high areal capacitance (831 F cm^{-2}), a high energy/power density (73.8 μWh cm^{-2} at 4960 μW cm^{-2}), and a capacitance retention of 86.5% after 1000 cyclic charging and discharging procedures. The PAAm matrix enables the supercapacitors to be flexible and bendable, allowing for 95% retention of capacitive performance after 5000 bending cycles. The rational design of the electrolyte matrix and electrode loading opens new opportunities for the design of novel high-performance materials for flexible energy storage applications.

3. Experimental Section

Chemicals: Acrylamide (Fisher, 98.0%), MBA (Fisher, 98%), PVA (molecular weight = 89 000–98 000, hydrolysis degree = 99%, Sigma), TEMED (99%, Fisher), APS (ACS grade, fisher), pyrrole (reagent grade, 98%, Sigma), iron(III) chloride hexahydrate (Sigma) were used. All chemicals were used as received.

Preparation of Precursor Solution: For the PVA precursor solution, 4 g PVA was dissolved in 40 mL water and heated to 90 °C with magnetic stirring to form a transparent solution with the PVA concentration of 10 wt%. The PVA solution was cooled down to room temperature for further usage. For the LiCl/PVA electrolyte solution, LiCl was added and mixed in 10 wt% PVA solution at 90 °C. Then, the solution was cooled down to room temperature to form 5 M LiCl/ PVA solution. For the hydrogel prepolymer solution, 1200 mg of acrylamide, 24 mg of MBA (as the crosslinker of acrylamide), 0.67 mL of ethanol, 40 μL of TEMED, and a certain amount of PVA solution were mixed to form solution A. To study the effect of PVA concentration on hydrogel morphology and supercapacitor electrochemical performance, 0, 0.5, 1, 2, and 3 wt% PVA was used. After mixing, the solution was degassed under nitrogen for 10 min to remove the dissolved oxygen. Solution B was prepared by adding 40 mg APS (as an initiator) in 1.33 mL water. The prepolymer solutions were kept at 4 °C fridge for further usage.

Preparation of the APA: The directional freezing mold was made of polylactic acid (PLA) with dimensions of 3 cm × 3 cm × 2.5 cm and 0.8 mm thick hollow side walls. For each sample, 5 mL of solution A and 0.33 mL of solution B were mixed and quickly transferred into the PLA mold. The bottom of the mold was immersed in liquid nitrogen with 1 mm depth, so that the bottom surface was always in contact with a cold source. The mold was fixed and the surrounding container with liquid nitrogen was gradually elevated with 10 μm s^{-1} to ensure the advancing ice front had sufficiently low temperature. As the ice grew to the top surface of the prepolymer solution, the mold was taken out of liquid nitrogen and kept in a −20 °C fridge for 3 h to complete the cryopolymerization of the PAAm hydrogel. The sample was subsequently freeze-dried for 2 days to remove the ice crystals and finally form an aligned PAAm aerogel (APA) film. The nonaligned, homogenous PAAm hydrogel (HomoPA) as the control sample was made by injecting prepolymer solution in a mold with defined thickness and placing in −20 °C fridge for polymerization.

Preparation of the PPy/APA Electrode: The APA film was sanding to the desired thickness with a sandpaper and cut to a desired size with a razor blade. Then, the film was immersed in a 14 w/v% $FeCl_3$-ethanol solution for 5 min. After drying in vacuum for 2 h, the film was placed in a vacuum desiccator with 1 mL of fresh pyrrole monomer. Under vacuum, the pyrrole monomer evaporated, deposited, and polymerized on the pore walls of APA aerogel with $FeCl_3$. Then the PPy/APA film was soaked in ethanol for 2 days to remove excessive reactants.

Assembly of All-Solid-State Supercapacitor: Two PPy/APA films with dimensions 1.27 cm × 1.27 cm × 1 mm were soaked in 5 M LiCl/ PVA aqueous solution for 1 day. Then a cellulose-based separator was sandwiched between two PPy/APA films and pressed together. The supercapacitor was kept in dry air for 15 h to form an integrated all-solid-state supercapacitor.

Characterizations: The morphology of the APA film was observed via scanning electron microscope (SEM, Supra 40VP) after freeze-drying. The electrochemical tests were performed via two-electrode method on a CHI660E electrochemical workstation (CH instrument). The CV measurements were examined at scan rates of 10, 20, 50, and 100 mV s^{-1}. The GCD curves were measured with various current densities in the potential range of 0–0.8 V. The EIS measurement was performed in the frequency range from 1 00 000 to 0.01 Hz, with a voltage perturbation of 5 mV. The cyclic stability test was performed by cyclic charging and discharging at a certain current density. The areal capacitance (C_A), the areal energy density (E_A), and the areal power density (P_A) of supercapacitor were calculated according to Equations (1), (2), and (3), respectively

$$C_A = \frac{2It}{AU} \tag{1}$$

$$E_A = \frac{C_A U^2}{2} \tag{2}$$

$$P_A = \frac{E_A}{t} \tag{3}$$

Supporting Information

Supporting Information is available from the Wiley Online Library or from the author.

Acknowledgements

The authors thank Qiulong Wei, Yeping Zhao, and Zipeng Zhao for the help with the basic electrochemical testing. The research was supported by the NSF Award 1724526, the ONR Award N000141712117, the ONR Award N00014-18-1-2314, the AFOSR Grant FA9550-17-1-0311, and the AFOSR award FA9550-18-1-0449.

Conflict of Interest

The authors declare no conflict of interest.

Author Contribution

X.H. conceived the concept, planned the project, and supervised the research. X.H., Y.Z., and S.W. designed and conducted the experiments and data analysis. Y.Z., Y.Z., B.Z., and N.B. conducted the fabrication and characterization. Y.Z., X.H., Y.A., and B.Y. wrote the manuscript.

Keywords

directional freezing, flexible, hydrogel, morphology control, supercapacitors

Received: November 3, 2019
Revised: December 10, 2019
Published online:

[1] E. Proksch, J. M. Brandner, J.-M. Jensen, *Exp. Dermatol.* **2008**, *17*, 1063.
[2] A. J. Sophia Fox, A. Bedi, S. A. Rodeo, *Sports Health: Multidiscip. Approach* **2009**, *1*, 461.
[3] Y. Zhang, W. Luo, C. Wang, Y. Li, C. Chen, J. Song, J. Dai, E. M. Hitz, S. Xu, C. Yang, Y. Wang, L. Hu, *Proc. Natl. Acad. Sci. U. S. A.* **2017**, *114*, 3584.
[4] K. Sano, Y. Ishida, T. Aida, *Angew. Chem., Int. Ed.* **2018**, *57*, 2532.
[5] H. Gu, R. Zheng, X. Zhang, B. Xu, *Adv. Mater.* **2004**, *16*, 1356.
[6] J. Xu, H.-C. Wu, C. Zhu, A. Ehrlich, L. Shaw, M. Nikolka, S. Wang, F. Molina-Lopez, X. Gu, S. Luo, D. Zhou, Y.-H. Kim, G.-J. N. Wang, K. Gu, V. R. Feig, S. Chen, Y. Kim, T. Katsumata, Y.-Q. Zheng, H. Yan, J. W. Chung, J. Lopez, B. Murmann, Z. Bao, *Nat. Mater.* **2019**, *18*, 594.
[7] Q. Fu, Y. Si, C. Duan, Z. Yan, L. Liu, J. Yu, B. Ding, *Adv. Funct. Mater.* **2019**, *29*. 1808234.
[8] Y. Wang, D. Kong, W. Shi, B. Liu, G. J. Sim, Q. Ge, H. Y. Yang, *Adv. Energy Mater.* **2016**, *6*, 1601057.
[9] W. Weng, H. Lin, X. Chen, J. Ren, Z. Zhang, L. Qiu, G. Guan, H. Peng, *J. Mater. Chem. A* **2014**, *2*, 9306.
[10] J. Billaud, F. Bouville, T. Magrini, C. Villevieille, A. R. Studart, *Nat. Energy* **2016**, *1*, 16097.
[11] J. S. Sander, R. M. Erb, L. Li, A. Gurijala, Y. M. Chiang, *Nat. Energy* **2016**, *1*, 16099.
[12] C. Chen, Y. Zhang, Y. Li, J. Dai, J. Song, Y. Yao, Y. Gong, I. Kierzewski, J. Xie, L. Hu, *Energy Environ. Sci.* **2017**, *10*, 538.
[13] Z. Zhao, R. Fang, Q. Rong, M. Liu, *Adv. Mater.* **2017**, *29*, 1703045.
[14] L. Li, Z. Lou, D. Chen, K. Jiang, W. Han, G. Shen, *Small* **2018**, *14*, 1702829.
[15] S. Lin, J. Liu, X. Liu, X. Zhao, *Proc. Natl. Acad. Sci. U. S. A.* **2019**, *116*, 10244.
[16] M. Liu, Y. Ishida, Y. Ebina, T. Sasaki, T. Hikima, M. Takata, T. Aida, *Nature* **2015**, *517*, 68.
[17] Q. Lu, S. Bai, Z. Ding, H. Guo, Z. Shao, H. Zhu, D. L. Kaplan, *Adv. Mater. Interfaces* **2016**, *3*, 1500687.
[18] H. Zhang, I. Hussain, M. Brust, M. F. Butler, S. P. Rannard, A. I. Cooper, *Nat. Mater.* **2005**, *4*, 787.
[19] W. Yang, H. Furukawa, J. P. Gong, *Adv. Mater.* **2008**, *20*, 4499.
[20] X. Liu, B. Wang, Z. Jin, H. Wang, Q. Wang, *J. Mater. Chem. A* **2015**, *3*, 15408.
[21] X. Liu, O. O. Taiwo, C. Yin, M. Ouyang, R. Chowdhury, B. Wang, H. Wang, B. Wu, N. P. Brandon, Q. Wang, S. J. Cooper, *Adv. Sci.* **2019**, *6*, 1801337.
[22] J. Wei, C. Yin, H. Wang, Q. Wang, *J. Mater. Chem. A* **2018**, *6*, 58.
[23] J. Lee, Y. Deng, *Soft Matter* **2011**, *7*, 6034.
[24] J. Wu, Q. Zhao, J. Sun, Q. Zhou, *Soft Matter* **2012**, *8*, 3620.
[25] M. Yang, J. Wu, H. Bai, T. Xie, Q. Zhao, T.-W. Wong, *AIChE J.* **2016**, *62*, 4186.
[26] J. Wu, Q. Zhao, C. Liang, T. Xie, *Soft Matter* **2013**, *9*, 11136.
[27] Q. Chen, H. Lu, F. Chen, L. Chen, N. Zhang, M. Ma. *ACS Appl. Energy Mater.* **2018**, *1*, 4261.
[28] K. Wang, X. Zhang, C. Li, X. Sun, Q. Meng, Y. Ma, Z. Wei, *Adv. Mater.* **2015**, *27*, 7451.
[29] K. Sun, E. Feng, G. Zhao, H. Peng, G. Wei, Y. Lv, G. Ma, *ACS Sustainable Chem. Eng.* **2018**, *7*, 165.
[30] K. Shen, J. Ding, S. Yang, *Adv. Energy Mater.* **2018**, *8*, 1800408.
[31] H. Liang, J. Lin, H. Jia, S. Chen, J. Qi, J. Cao, Y. Lin, W. Fei, J. Feng, *J. Power Sources* **2018**, *378*, 248.
[32] L. Zang, Q. Liu, J. Qiu, C. Yang, C. Wei, C. Liu, L. Lao, *ACS Appl. Mater. Interfaces* **2017**, *9*, 33941.
[33] P. Zhang, J. Li, L. Lv, Y. Zhao, L. Qu, *ACS Nano* **2017**, *11*, 5087.
[34] D. Chen, Y. Zhang, C. Ni, C. Ma, J. Yin, H. Bai, Y. Luo, F. Huang, T. Xie, Q. Zhao, *Mater. Horiz.* **2019**, *6*, 1013.
[35] R. C. Deller, M. Vatish, D. A. Mitchell, M. I. Gibson, *Nat. Commun.* **2014**, *5*, 3244.
[36] M. C. Gutiérrez, Z. Y. García-Carvajal, M. Jobbágy, F. Rubio, L. Yuste, F. Rojo, M. L. Ferrer, F. del Monte, *Adv. Funct. Mater.* **2007**, *17*, 3505.
[37] C. Guan, X. Li, Z. Wang, X. Cao, C. Soci, H. Zhang, H. J. Fan, *Adv. Mater.* **2012**, *24*, 4186.
[38] Z. Gu, Y. Xu, L. Chen, R. Fang, Q. Rong, X. Jin, L. Jiang, M. Liu, *Macromol. Mater. Eng.* **2018**, *303*, 1800339.
[39] Q. Dou, Z. W. K. Low, K. Zhang, X. J. Loh, *RSC Advances* **2017**, *7*, 27449.
[40] W. Wei, X. Hu, X. Qi, H. Yu, Y. Liu, J. Li, J. Zhang, W. Dong, *Colloids Surf., B* **2015**, *125*, 1.
[41] H. Li, T. Lv, N. Li, Y. Yao, K. Liu, T. Chen, *Nanoscale* **2017**, *9*, 18474.
[42] R. Buitrago-Sierra, M. J. García-Fernández, M. M. Pastor-Blas, A. Sepúlveda-Escribano, *Green Chem.* **2013**, *15*, 1981.
[43] F. Chen, Q. Chen, Q. Song, H. Lu, M. Ma, *Adv. Mater. Interfaces* **2019**, *6*, 1900133.
[44] H. Zhou, G. Han, Y. Xiao, Y. Chang, H.-J. Zhai, *J. Power Sources* **2014**, *263*, 259.
[45] B. Yao, L. Yuan, X. Xiao, J. Zhang, Y. Qi, J. Zhou, J. Zhou, B. Hu, W. Chen, *Nano Energy* **2013**, *2*, 1071.
[46] H. Zhou, H.-J. Zhai, *Org. Electron.* **2016**, *37*, 197.
[47] X. Zang, X. Li, M. Zhu, X. Li, Z. Zhen, Y. He, K. Wang, J. Wei, F. Kang, H. Zhu, *Nanoscale* **2015**, *7*, 7318.
[48] Y. Fu, H. Wu, S. Ye, X. Cai, X. Yu, S. Hou, H. Kafafy, D. Zou, *Energy Environ. Sci.* **2013**, *6*, 805.
[49] S. E. Moosavifard, M. F. El-Kady, M. S. Rahmanifar, R. B. Kaner, *ACS Appl. Mater. Interfaces* **2015**, *7*, 4851.